Influence of growth temperature variation of Cr_2O_3 thin film on nonlinear optical characterization

Ali M. Ibrahim[1,2], Elham H. El-Anssary[1,2,*], Ayman El-Amin[1,2]

[1]Physics Department, Faculty of Science, Aswan University, Aswan, 81528, Egypt.

[2]Research Centre for Nano-Material Studies and their Promising Technologies, Aswan University, Aswan, Egypt.

Abstract

This study discussed the effect of temperatures on the structural and optical properties of the Cr_2O_3 thin films. Thin films of Cr_2O_3 were deposited using the spray pyrolysis technique with different growth temperatures. The primary solution of 0.1 mole was sprayed on glass substrates at 250,350, and 450 ˚C using air as the carrier gas. According to XRD, SEM, and Visible - UV optical spectroscopy measurements, the samples were characterized by a polycrystalline structure and distinctive optical properties of thin films. The XRD analysis confirmed the hexagonal structure of thin films, and the average crystallite size of the samples prepared at the highest temperature (450 °C) is 13.17 nm. Scanning electron microscopy (SEM) illustrated the morphology of coated samples and showed the spherical configuration of crystals. These samples exhibit a direct band gap, and the band gap energy increased from 2.47585 at 250 °C to 3.0343 eV at 450 °C.

Keywords: Cr_2O_3; nanoparticles; thin film; spray pyrolysis; direct band gap.

1. Introduction

In recent years, nanoscience and nanotechnology have significantly increased their application within scientific research. Nanoscience and nanotechnology encompass the study, manipulation, and implementation of materials, phenomena, and devices at nanometer dimensions—typically less than 100 nanometers. At this scale, the fundamental behavior of materials often deviates from classical laws and instead adheres to quantum mechanics. This results in novel mechanical, electrical, optical, thermal, and chemical properties **[1]**. Among the most prominent nanostructures are thin films, which are classified as two-dimensional materials—such as nanolayers and nanosheets—due to their extremely small thickness and extended lateral dimensions. Their distinct characteristics make them ideal candidates for a wide range of advanced technological applications **[2]**.

Metal oxides have excellent features and have a huge number of applications in numerous areas, including gas sensors, optoelectronics, electrochemistry, microelectronics, optics, p-type transparent conducting oxides, hydrogen storage, catalysts, buffer layers in organic solar cells, wear resistance materials, and other Fields **[3-8]**. Metal oxides are of two kinds, namely: i) Transition metal oxides and ii) Non-transition metal oxides **[9]**. Transition metal oxides have gained significant attention in environmental technologies owing to their adaptable chemical composition, adjustable bandgaps, natural abundance, promising optoelectronic characteristics, responsiveness to visible light, and stable catalytic performance. Among them, Cr_2O_3 stands out as a representative material, offering a tunable optical bandgap and strong visible-light absorption, making it highly suitable for applications in photocatalysis and optoelectronics **[10]**.

*Corresponding author E-mail: elham_alanssary@aswu.edu.eg

Received May 27, 2025, received in revised form, August 10, 2025, accepted August 11, 2025.

(ASWJST 2021/ printed ISSN: 2735-3087 and on-line ISSN: 2735-3095) https://journals.aswu.edu.eg/stjournal

Chromium (III) oxide (Cr_2O_3) is one of the transition metal oxides with specified material properties of technological importance and is extensively researched due to its attractive physical and chemical properties. Among chromium oxides (Cr_2O, Cr_3O_4, CrO, CrO_2, CrO_3, Cr_8O_{11}), chromium sesquioxide (Cr_2O_3) exhibits the greatest stability **[11-14]**. Cr_2O_3 has been the main subject of several types of studies and research, especially in thin layers due to its unique properties and its extensive use in industrial applications, and concurrently, thin film applications possess great interest because of their wide variety of technological uses **[12]**. The high hardness, corrosion resistance, and selective absorption film properties of Cr_2O_3 are raising significant concerns. Chromium oxide (Cr_2O_3) demonstrates significant potential for various advanced applications due to its strong nonlinear optical properties. Its nonlinear absorption makes it a promising material for use in nonlinear optical devices and into photonic and optoelectronic systems. Additionally, Cr_2O_3's excited-state interactions render it suitable for laser-based technologies and optical switching applications **[15]**.

Cr_2O_3 raises significant concern because it shows high hardness and corrosion resistance and perfect selective absorption films for converting solar energy, which was explained by studying thin films' electrical and optical properties. Its unique contribution to electronics includes applications in solar energy harvesting, sensor development, and photocatalysis **[16, 17].** Chromium Oxide thin films have been prepared using various techniques, including spin coating, pulsed laser deposition, thermal evaporation, e-beam evaporation, and spray pyrolysis deposition **[12, 13, 18-20]**. In previous study, it was reported that Cr_2O_3 thin films exhibit a tunable optical band gap ranging from 2.70 to 2.99 eV. This variation is influenced by the oxygen content during deposition, making the material suitable for adjustable optoelectronic applications **[21]**. Another study reported that the optical band gap of pure Cr_2O_3 was reported as 3.0 eV, measured using UV–Vis spectroscopy and Tauc plot analysis **[22]**. The optical band gap of Cr_2O_3 thin films prepared by pneumatic spray pyrolysis was found to decrease from 3.53 eV to 3.38 eV with increasing precursor concentration, depending on the type of chromium salt used **[23]**. While the Urbach energy values for Cr_2O_3 thin films prepared by pneumatic spray using the chromium nitrate ($Cr(NO_3)_3$) precursor were reported to decrease fromo.97 to 0.68 eV as the solution concentration was decreased, indicating growing disorder in the film structure **[23]**. Tauc plot analysis of green-synthesized Cr_2O_3 nanoparticles, using Opuntia dillenii extract, reveals a direct optical band gap near 2.93 eV, according to Muzammal et al. [24]. This value shows significant visible-light absorption, making them suitable for photocatalysis and optoelectronics **[24]**.

In the present study, spray pyrolysis was employed to deposit Chromium Oxide thin films onto glass substrates **[25, 26]**. This technique is widely recognized for its simplicity and effectiveness in producing films of varying thicknesses. The setup of the spray pyrolysis technique includes an atomizer, a substrate heater, a temperature controller, and a precursor solution reservoir (steering pump). During deposition, the atomizer generates a fine mist of the precursor solution, which reacts upon contact with the heated substrate to form the chemical compound. The impact of substrate temperature on the structural and optical properties of the films was systematically investigated.

2. Experimental

2.1 Materials and methods

The spray pyrolysis technique synthesized *(Cr_2O_3)* thin films. Before the deposition of thin films, the glass substrates were chemically cleaned in distilled water and soap, then washed with deionized water before being left in action, Finally, the substrates were dried in a drying oven at 100 °C. Pure Chromium(III)Chloride Hexahydrate (*$CrCl_36H_2O$,* Sigma-Aldrich) was used as a single source of Chrome and oxygen for the deposition of sprayed *Cr_2O_3* thin films. For preparing the starting solution, 0.7994 g of *$CrCl_36H_2O$* was dissolved in 30 mL of deionized water, and this aqueous solution was continuously stirred for 15 min at 500 rpm until a homogenous clear solution was achieved. Thus, a 0. 1M precursor solution was prepared for performing the *Cr_2O_3* films deposition. The SP technique was optimized extensively before these films were spray deposited. Spray parameters were controlled by a separate control box, where several conditions influenced spray deposition. The nozzle and hot plate separation distance was adjusted to 30 cm, and air pressure was set to 3.5 bar. In contrast, the spray time and interval time were set at 4 and 10 seconds for 350 seconds continuously to perform *(Cr_2O_3)* thin films consisting of 25 layers. Three thin film samples were produced by adjusting the hot plate temperature at 250, 350, and 450 °C while maintaining optimal settings for all other spray parameters. The film structure relies primarily on three parameters: precursor solution concentration, the number of deposition cycles and the temperature of the substrate hot plate. Herein, different temperatures were performed on the substrate hot plate, while other parameters remained constant to study the impact of temperature on the structural, morphological, and optical properties.

2.2 Characterization techniques

The structural analysis of deposited films was performed using an X-ray diffractometer (Bruker D8 Advance) using *Cu* kα monochromatic radiation (λ = 1.5406 Å). While studying the morphology of the particles in the thin films applied using scanning electron microscopy (SEM). On the other hand, the optical properties of the *Cr_2O_3* sprayed thin films were studied using a spectrophotometer model UV-Vis-NIR JASCO V-670.

3. Results and discussion

3.1. Structural characterization

3.1.1 (X-Ray Diffraction)

The XRD patterns shown in Fig.1 are of *Cr_2O_3* films made by spray pyrolysis at different temperatures. Samples deposited at 250˚C, 350˚C, and 450˚C showed a substantial correlation between temperature and crystallinity, where the increase in the degree of crystallinity was observed significantly for samples with the increase in growth temperature. The X-ray diffraction pattern of *Cr_2O_3* thin films showed at the temperature of 250˚C a weak reflex at 2theta values 36.19, 39.93, 41.59, and 55.01, followed by an increase in crystallization with the rise of growth temperature to 350˚C. As a result, the appearance of strong peaks at 2ϑ = 33.872˚, 36.562˚, 39.93˚, 41.89˚and 55.32˚, as shown in Fig.1. while appearing of new peaks at 22.556, 40.07˚, 50.595˚, and 65.525˚. At growth temperature 450˚ C, there was a displacement for peaks 22.556˚ to 24.56˚and 39.93˚ to 40.070˚, which matched perfectly with the standard JCPDS card of *Cr_2O_3*

number 00–038–1479. The intensity of peaks increased, and this confirmed the increase in crystallization. peaks of XRD pattern (24.56˚, 33.872˚, 36.562˚, 40.070˚,50.674˚, 55.32˚, and 65.551˚) correspond respectively to (012), (104), (110), (006), (113), (024), and (116) planes. These reflections are the fingerprints of the Cr2O3 crystalline lattice structure, which are attributed to the hexagonal structure of Cr_2O_3.

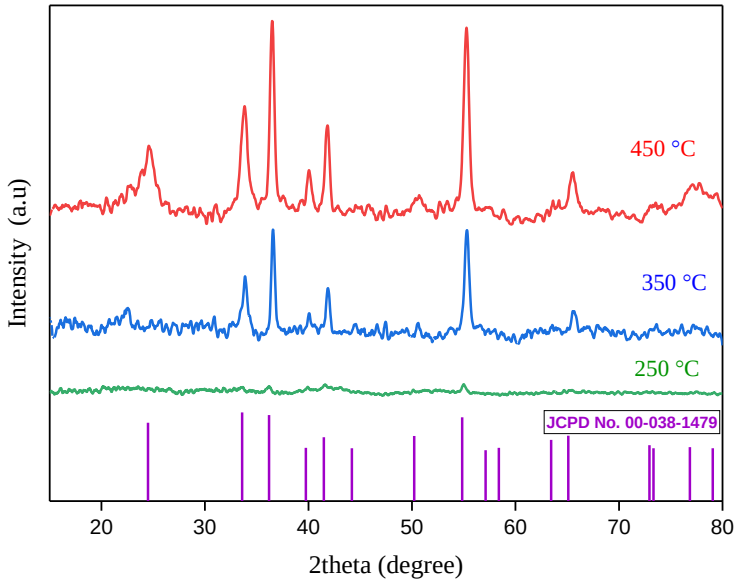

Fig.1. XRD patterns of the Cr_2O_3 thin films at different growth temperatures, compared to the card (JCPDG No. 00-038-1479) of Cr_2O_3 nanocrystal.

The average crystal size was calculated using the Debye-Sherrer equation **[27, 28]**: -

$$D = \frac{k\lambda}{\beta\cos\theta} \qquad (1)$$

Where K = 0.9; Sherrer constant, λ = 0.15406 nm; is the wavelength of the X-ray source, β full width half maximum, θ is the peak position, and D is the crystallite size. Here, the crystal size can be controlled by controlling the number of film layers sprayed by spray pyrolysis.

Table.1 shows the change in crystal size of deposited Cr_2O_3 thin film with various growth temperatures, and this indicates that the growth temperature of the spray pyrolysis technique is the dominant factor controlling grain size.

Table.1

Growth temperature˚ C	Crystallinity ratio	Average value of crystallite size
250	15.1897	15.373
350	45.34485	14.98902
450	67.78988	13.17151

The crystallinity ratio of samples, as shown in Table.1 was determined using the following equation **[29]**:

$$\text{Crystallinity ratio} = \frac{\text{area of crystalline peaks}}{\text{area of all peaks}} * 100 \qquad (2)$$

The values from Table.1 establish the significant effect of growth temperature on the crystallinity of Cr_2O_3 thin films.

3.1.2 SEM analysis

Fig.2 shows the SEM images of (Cr_2O_3) thin film at different magnification degrees taken by scanning electron microscopy, which was deposited onto a glass substrate by spray pyrolysis at a hotplate temperature of 450˚C by using a precursor solution with a concentration of 0.1M, and the result is that the thin film consists of 25 layers. The morphology of the *(Cr_2O_3)* calcined at 450̊ °C displays a fantastic uniform distribution, as obvious in Fig.2. The deposited *(Cr_2O_3)* film exhibited quasi-spherical-shaped particles (spherical and ellipsoidal) with an average particle size of 191 nm. The nanoparticles are in the form of clusters with some distance in between. The distribution is more granular, and it shows uniformity in particle size.

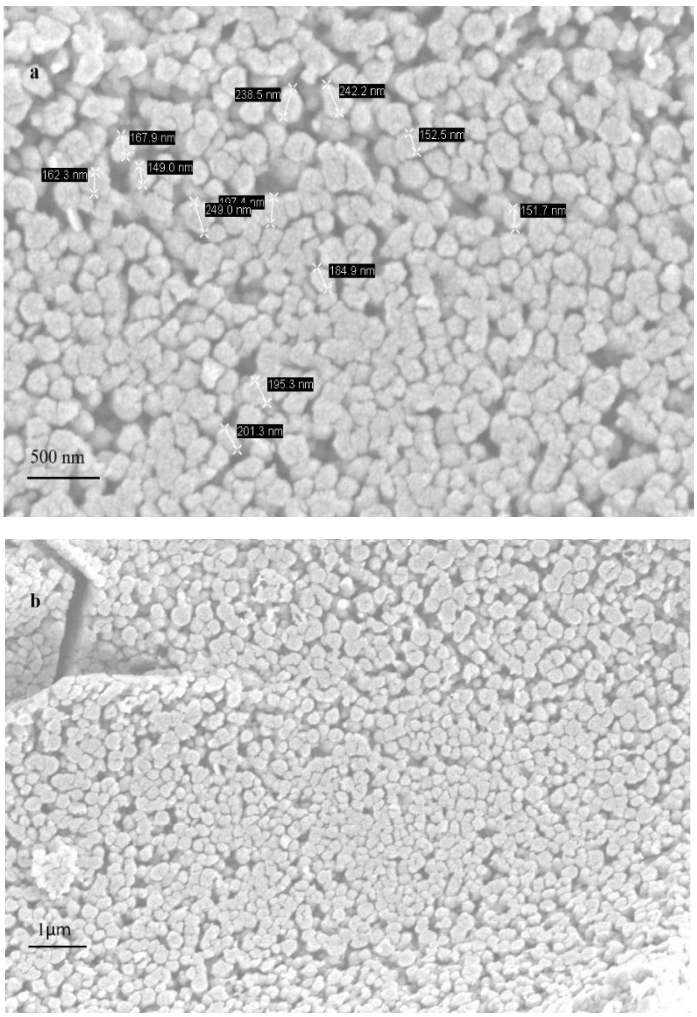

Fig.2. SEM images of the Cr_2O_3 thin films at 450̊ C growth temperature, **a**(500 nm)**,b**(1µm).

3.2. Optical spectroscopy

UV/vis/NIR spectroscopy is very useful for the optical analysis of nanomaterials. Figs. 3 and 4 depict the optical transmittance and absorbance spectra of deposited (Cr_2O_3) thin films within the 200–1700 nm wavelength range. Fig.3 shows a dramatic increase in the transmission of samples by increasing growth temperature, especially in the visible spectrum range from 300 nm to 750 nm. A significant increase in the transmittance, explained by this, confirms the XRD result of crystal size **[30]**. The increase in transmittance is met with a decrease in absorption **[31]**, as shown in Fig.4 for the same region.

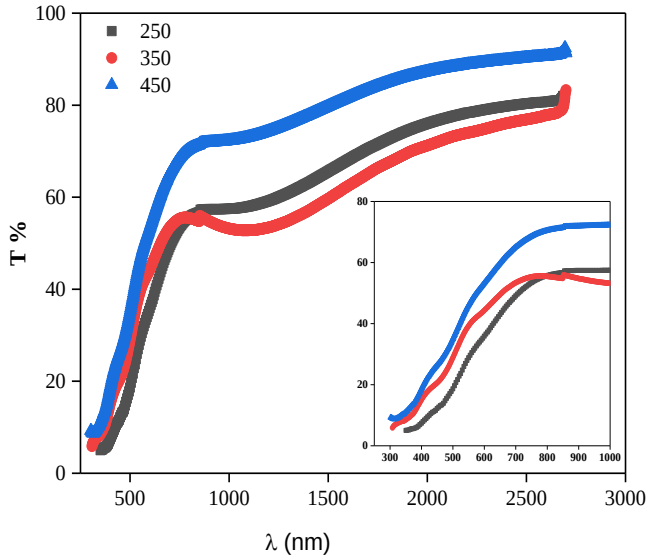

Fig. 3. The transmittance spectra of Cr_2O_3 thin films grown at different growth temperatures

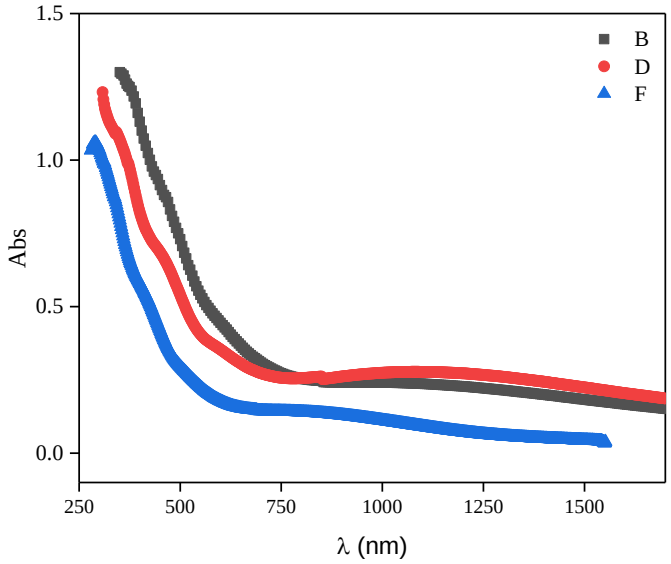

Fig. 4. The absorbance spectra of Cr_2O_3 thin films grown at different growth temperatures

In the present work, the absorption coefficient (α) was determined, based on the transmission spectra (T) and the film thickness (t) as described below **[32]**.

$$\alpha = \frac{1}{d}.\ln(\frac{1}{T}) \qquad (3)$$

The absorption coefficient (α) is the key to calculating the energy gap (Eg), which is the basic feature of the optical spectra measurement, and it is determined by:

$$\alpha = \frac{1}{h\upsilon}[B(h\upsilon - Eg)^n] \qquad (4)$$

Where hυ is the photon energy, the transition probability is estimated by the constant *B, and* the exponent *n* is an index that characterizes the type of optical transition occurring in the film sample. The value of *n* is equal to 2, 1/2, 3, or 3/2 for the indirect allowed, direct allowed, indirect forbidden, or direct forbidden transitions, respectively **[33, 34]**. At the exponent *n=1/2 and* through the following formula:

$$(\alpha h\upsilon)^2 = B(h\upsilon - Eg) \qquad (5)$$

From this relation between $(\alpha h\upsilon)^2$ and $h\upsilon$, through extrapolating the linear portion of the curve, the optical band gap can be estimated, where it intersects the x-axis of photon energy. The Tauc plots for all deposited (Cr_2O_3) nanostructured thin films are shown in Fig.5 with different growth temperatures and a direct band gap. Tauc plots are fitted by the variation of the quantity $(\alpha h\upsilon)^2$ as a function of the photon energy. The values of optical band gap energies (in eV) are 2.476, 2.762, and 3.034 for samples 250,350, and 450, respectively. A direct correlation exists between optical band gap and growth temperature; this is explained as a result of the decline in crystallite size with the increase in growth temperature. These findings lead us to conclude that the band gap energy increases as the crystallite size decreases and this can be attributed to the quantum confinement effect which occurs in nanomaterials when the size of the crystallite becomes comparable to or smaller than the material's exciton Bohr radius **[35, 36].**

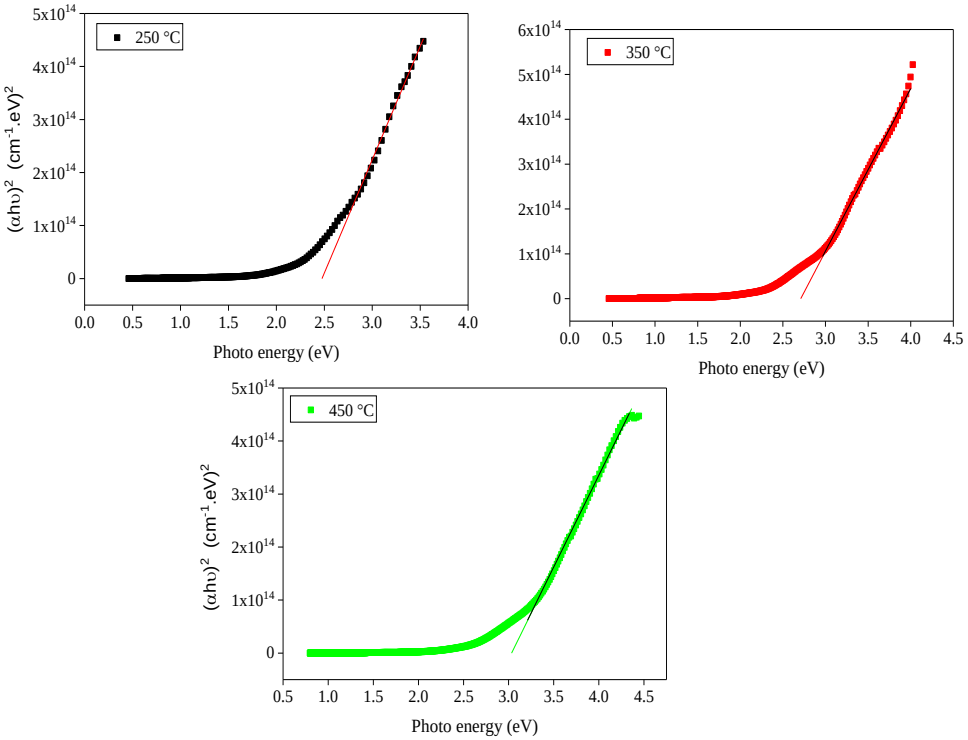

Fig. 5. Tauc plot of Cr_2O_3 thin films grown at different growth temperatures.

Urbach energy is a function of defect states between the conduction and the valence bands. Urbach energy at a specific temperature is determined by the relationship between the optical absorption coefficient and incident photon energy **[37]**:

$$\ln(\alpha) = \frac{1}{\mathrm{Eu}}(h\upsilon) + \ln(\alpha_0) \qquad (6)$$

Where (α_0) is a constant; the incident photon energy is $h\upsilon$ while Eu is the Urbach energy ascribed as a width of the band tail of localized states in the band gap. Fig.6. shows the linear relation between the optical absorption coefficient (α) and the incident photon energy Fig. 6. demonstrates a linear correlation between the optical absorption coefficient (α) and the incident photon energy, where the Urbach energy is determined from the inverse slope of the linear region of the exponential curve. A slight decrease in Urbach energy with increasing growth temperature was observed, indicating a direct relationship between Urbach energy and crystallite size. This trend is further supported by Fig. 7. which highlights an inverse relationship between the optical

band gap and crystallite size, with a clear direct correlation between crystallite size and Urbach energy. These findings collectively confirm an inverse correlation between Urbach energy and band gap energy, both of which are significantly influenced by changes in crystallite size as a function of the deposition temperature. In light of these results, the observed increase in band gap energy (Eg) suggests enhanced crystallinity and reduced structural disorder, which consequently leads to a lower Urbach energy (Eu), reflecting the improved quality of the thin film **[38]**. Understanding these correlations is essential for tailoring the optical properties of Cr_2O_3 thin films to suit specific applications. Given the observed nonlinear optical behavior and optical properties, these films exhibit strong potential for use in optoelectronic and photonic devices as photovoltaics, laser diodes devices.

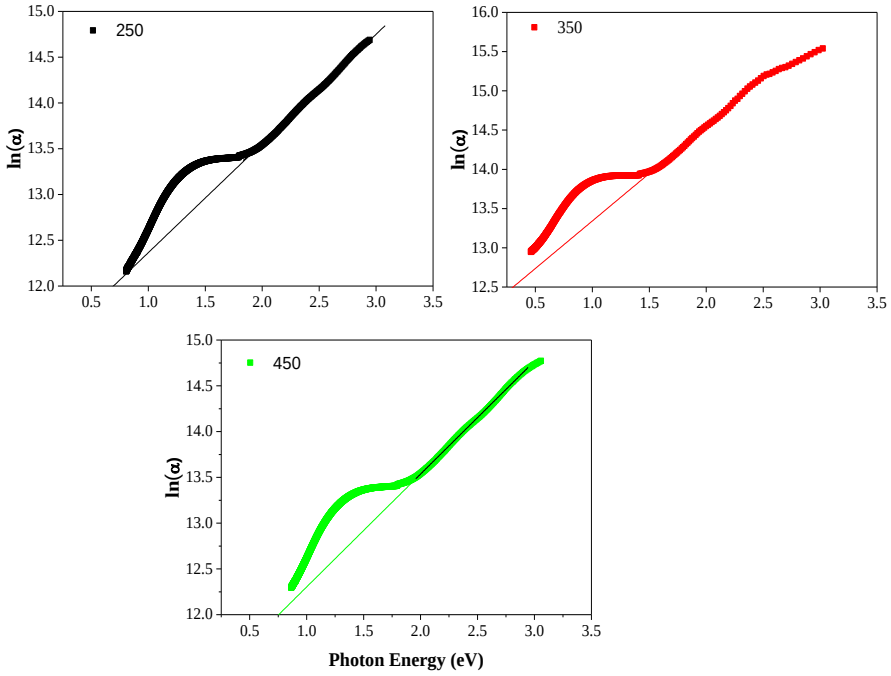

Fig. 6. The relation of ln(α) against the photon energy for Cr_2O_3 thin films grown at different temperatures to determine Urbach energy.

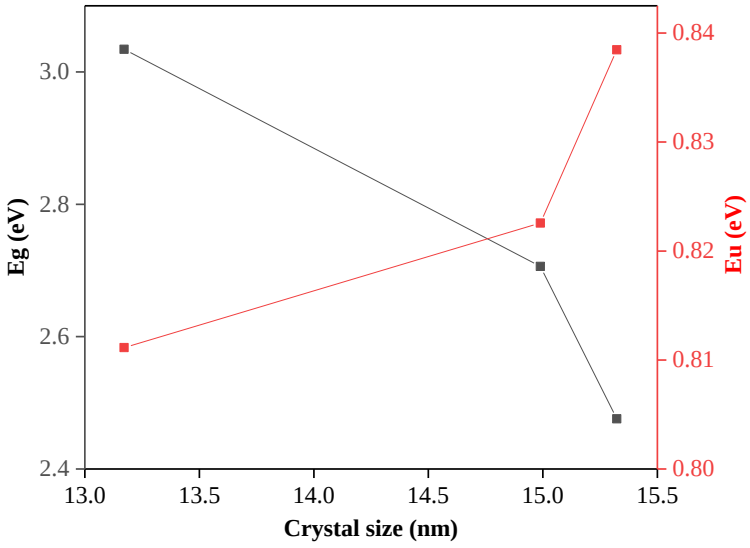

Fig. 7. The dependence of band gap energy and Urbach energy on the crystal size of deposited thin films.

4. Conclusion:

This work reports the successful fabrication of Cr_2O_3 nanoparticle thin films using an affordable and straightforward spray pyrolysis technique. Structural analysis via X-ray diffraction (XRD) confirmed the polycrystalline nature of the films synthesized at different growth temperatures. Morphological examination using scanning electron microscopy (SEM) revealed quasi-spherical nanoparticles. Variations in growth temperature were found to significantly influence both the intensity of the XRD peaks and the degree of crystallinity. The estimated crystallite sizes ranged from 13.17nm to 15.32 nm and the crystallinity ratio improved to become 67.78988% at growth temperature 450 ˚C. Optical measurements indicated an increase in the optical band gap to 3.034 eV with temperature. The Urbach energy exhibited a slight decrease from 0.84 to 0.81 eV, suggesting an inverse correlation of band gap energy with the crystallite size and Urbach energy. These structural and optical properties highlight the potential of Cr_2O_3 nanoparticle films for applications in photovoltaics, laser diodes, and optoelectronic devices.

References:

1. Baig, N., I. Kammakakam, and W.J.M.a. Falath, *Nanomaterials: A review of synthesis methods, properties, recent progress, and challenges. Royal Society of Chemistry* 2021, **2**(6), 1821-1871.
2. Kamal, A., Li, Baosong, Solayman, A., et al., *Mechanical properties of two-dimensional material-based thin film*s: a comprehensive review. *Royal Society of Chemistry* 2025, 10, 512-536
3. Dey, A.J.M.S. and E.B., *Semiconductor metal oxide gas sensors: A review. Materials Science and Engineering: B* 2018, 229, 206-217.
4. Yu, X., T.J. Marks, and A.J.N.M. Facchetti, *Metal oxides for optoelectronic applications. Nature Materials* 2016. 15(4), 383-396.
5. Yu, X.-Y., Z.-G. Liu, and X.-J.J.T.i.E.A.C. Huang, *Nanostructured metal oxides/hydroxides-based electrochemical sensor* for monitoring environmental micropollutants. *Trends in Environmental Analytical Chemistry* 2014. 3, 28-35.
6. Bhardwaj, P., Singh, J., Singh, A. P. et al., Observation of room temperature ferromagnetism in transition metal ions substituted p-type transparent conducting oxide Cr2O3 thin films. *Materials Science and Engineering: B 2024. 299.*
7. Bumajdad, A., et al., *Non-noble, efficient catalyst of unsupported α-Cr2O3 nanoparticles for low temperature CO Oxidation. Scientific Reports* 2017. **7**(1), 14788.
8. Qin, P., Fang, G., He, Qin, et al., Nitrogen doped amorphous chromium oxide: Stability improvement and application for the hole-transporting layer of organic solar cells. *Solar Energy Materials and Solar Cells* 2011. 95(3), 1005-1010.
9. Rao, C.N.R. and G.S. Rao, Transition metal oxides: crystal chemistry, phase transition, and related aspects.*National Institute of Standards and Technology (NIST)* 1974.
10. Okpara, E.C., Olatunde, O., C., Wojuola, Olanrewaju B., et al., Applications of transition metal oxides and chalcogenides and their composites in water treatment: a review. *Environmental Advances* 2023, 11,100341.
11. Ishtiaq, M., Ali, D., Ahmad, R. et al., Tuning optical and electrical characteristics through Cu doping in spray pyrolysis fabricated Cr2O3 thin films. *Optical Material* 2024, 148.
12. Kadari, A., Schemme, T., Kadri, D., et al., XPS and morphological properties of Cr2O3 thin films grown by thermal evaporation method. *Results in Physics* 2017, 7, 3124-3129.

13. Bermudez, V., and DeSisto, WJ., Study of chromium oxide film growth by chemical vapor deposition using infrared reflection absorption spectroscopy. *Journal of Vacuum Science Technology A*: 2001. 19(2) 576-583.
14. Gao, Y., Leiste, H., Stueber, M., et al., The process of growing Cr2O3 thin films on α-Al2O3 substrates at low temperature by r.f. magnetron sputtering. *Journal of Crystal Growth* 2017, 457, 158-163.
15. Alattar, A.S., Nadafan, M., Dehghani, Z., et al., Influence of d-d transition electrons and thickness variations on the excited-state optical properties: Nonlinear optical characterization of Cr_2O_3 thin film. *Journal of Luminescence* 2025, 277.
16. Saha, C.N., *Fabrication of Micron-Scale Test Structures for Magneto-Electric Chromia (Cr2O3) Thin Films*. 2020, State University of New York at Buffalo.
17. Mohamed, R.M., Ismail, A. A., and Alhaddad, M., A novel design of porous Cr2O3@ ZnO nanocomposites as highly efficient photocatalyst toward degradation of antibiotics: a case study of ciprofloxacin. Separation and Purification Technology 2021, 266, 118588.
18. Demirci, E., Öztürk, M.Öcal, M. T., et al., Investigation of spin canting phenomena in perpendicularly exchange biased Pt/Co/Pt/Cr2O3 thin films. *Thin Solid Films* 2015, 591, 72-75.
19. Ekinci, H., Soltani, M., Jahed, N. M. S., et al., Effect of annealing on the structural, optical and surface properties of chromium oxide (Cr_2O_3) thin films deposited by e-beam evaporation for plasma etching applications. *Journal of Alloys and Compounds* 2021, 875.
20. Panda, A.K., Singh, A., Divakar, R., et al., Crystallographic texture study of pulsed laser deposited Cr_2O_3 thin films. *Thin Solid Films* 2018, 660, 328-334.
21. Jagadish, K. and D.J.M.R.E. Kekuda, Performance evaluation of p-type Cr_2O_3 thin films grown by reactive DC magnetron sputtering for Schottky diode applications. *Materials Research Express* 2024. 11(10), 105901.
22. Alshammari, M., Alshammari, K., Alhassan, S. et al., *A high-performance Cr_2O_3/$CaCO_3$ nanocomposite catalyst for rapid hydrogen generation from NaBH4. Multidisciplinary Digital Publishing Institute (MDPI)* 2024, 14(4), 333.
23. Saadi, B., Rahmane, Saâd Laidoudi, Mouloud et al., Influence of concentration of different chemical precursors on the physical properties of Cr_2O_3 thin films elaborated via pneumatic spray. *Sage Journal* 2023, 22(1), 93-103.
24. Muzammal, S., Ali, S., Awais A. et al., Eco-friendly Cr_2O_3 nanoparticles from Opuntia dillenii for visible-light photocatalysis and antimicrobial defense against waterborne pathogens. *Ceramics International.* 2025 51(4), 5159-5167.
25. Perednis, D., Gauckler, and Lu. J., Thin film deposition using spray pyrolysis. Journal of Electroceramics, *Springer Nature,* 2005. 14 103-111.
26. Narwade, S.H., V.V. Jadhav, and R.S. Mane, Spray-pyrolysis technique for the synthesis of metal oxide nanostructures. *Solution Methods for Metal Oxide Nanostructures* 2023,155-174, Elsevier.
27. Fatimah, S., Ragadhita. R., Dwi Fitriaet, et al., How to calculate crystallite size from X-ray diffraction (XRD) using Scherrer method. *ASEAN Journal of Science and Engineering (AJSE)* 2022. 2(1),65-76.
28. Uvarov, V., and Popov, I., Metrological characterization of X-ray diffraction methods for determination of crystallite size in nano-scale materials. *Journal of Materials Characterization 2007, 58(7), 883-891.*
29. Abdul Mannana*, K.R.K., Muhammad Shafiq Khanb and I. H. Khana, A Method for the Determination of Relative Crystallinity of Minerals by X-Ray Diffraction. *Pakistan Journal of Scientific & Industrial Research*, 2006, 49(2), 72-76.

30. O, Y.T., Koo, J. B., Hong, K. J., et al., Effect of grain size on transmittance and mechanical strength of sintered alumina. *Materials Science and Engineering: A* 2004, 374(1-2), 191-195.
31. Smith, R.H.W.a.J.B., Transmittance, Reflectance, and Absorptance of Near Infrared Radiation in Textile Materials. *Textile research journal*, 1949.
32. Badr, A.M., Afify, H. H., Elham.H. El-Anssary et al., *Photochromic Response and Steady-State Photoconductivity of Fibrous-Reticulated α-MoO3 Thin Films Prepared by Modified Spray Pyrolysis Technique. Crystal Research and Technology,* 2019, 54(10).
33. Biswajit Choudhury* and M.D.a.A.C., *Defect generation, d-d transition, and band gap reduction in Cu-doped TiO2 nanoparticles.* International Nano Letters 2013, 3, 8.
34. Md. Julkarnain, J.H., Khairul Alam Khan, Optical properties of thermally evaporated Cr2O3 thin films. *Canadian Journal on Chemical Engineering & Technology* 2012, 3(4).
35. Sherka, G.T. and H.D.J.F. P. Berry, Insight into the impact of size and shape on optoelectronic properties of InX (X=As, Sb, and P) semiconductor nanoparticles: a theoretical study. *Frontiers in Physics 2024*. 12, 1447997.
36. Sadia, S.I., Shishir, Md., Khalid H.A. et al. Crystallographic biography on nanocrystalline phase of polymorphs titanium dioxide (TiO_2): A perspective static review. *Frontiers in Physics* 2024. 50(1), 51-64.
37. Singh, J., Verma, V., Kumar, R., et al., Effect of structural and thermal disorder on the optical band gap energy of Cr_2O_3nanoparticles. *Materials Research Express* 2019, 6(8).
38. Bouderbala, I. Y., Guessoum, Amir R., et al. "Optical band-diagram, Urbach energy tails associated with photoluminescence emission in defected ZnO thin films deposited by sol–gel process dip-coating: effect of precursor concentration. *Korea-Australia Rheology Journal* 2024, 130(3), 205.